A neuroendocrine principle: Pancreatic islets actively shape sympathetic innervation

Authors:

Dong-Xue Li[1,†], Jia-Mei Luo[1,†], Jun-Jie Wang[1,†], Yun-Zhen Qian[1,†], Dilinazi Abudujilile[1,†], Musitaba Mutailifu[1], Tian Yang[1], Yuan-Xin Hong[1], Wen-Tao Shi[1], Xiao-Yi Ma[1], Qing Ye[1], Lei Zhu[1], Hui-Li[1], Xiao-Mei Yang[1], Yan-Li Zhang[1], Shu-Heng Jiang[1], Yan-Qiu Yu[2], Kai Wang[3], Jun Li[1], Qing Li[1], Li-Peng Hu[1,*], Xue-Li Zhang[1,*], Zhi-Gang Zhang[1,*]

Affiliations:

[1] State Key Laboratory of Systems Medicine for Cancer, Shanghai Cancer Institute, Ren Ji Hospital, School of Medicine, Shanghai Jiao Tong University, Shanghai, China.

[2] Department of Pathophysiology, Basic Medical College, China Medical University, Shenyang, China

[3] Department of Physiology and Pathophysiology, School of Basic Medical Sciences, Peking University, Beijing, China

[†]Dong-Xue Li, Jia-Mei Luo, Jun-Jie Wang, Yun-Zhen Qian and Dilinazi Abudujilile contributed equally to this work.

*Corresponding authors: Zhi-Gang Zhang, E-mail: zzhang@shsci.org; or Xue-Li Zhang, E-mail: xlzhang@shsci.org; or Li-Peng Hu, E-mail: lphu@shsci.org

Abstract

Survival critically depends on maintaining blood glucose levels to provide essential energy, especially during emergencies such as the fight-or-flight response, when timely glucose control via neural integration is vital. However, pancreatic islets constitute only a small fraction of the pancreas and are dispersed throughout the organ, raising the fundamental question of how the nervous system coordinates synchronized control of multiple islets. Using whole-organ clearing and 3D imaging, we mapped pancreatic sympathetic innervation, revealing specialized anatomical integration between sympathetic nerves and islets. Transplanted islets intrinsically attracted sympathetic nerves independent of their native environment. Chronic islet injury disrupted sympathetic innervation and markedly impaired nerve regeneration after denervation. Sympathetic denervation markedly elevated islet-derived Reg2 and Reg3β; administration of these proteins accelerated sympathetic regeneration and improved islet graft function. Our findings identify an islet-sympathetic architecture actively maintained by islets, uncovering an endocrine-driven mechanism for neural regulation, highlighting Reg2 and Reg3β as therapeutic candidates for diabetes management.

Introduction

Precise coordination between the nervous and endocrine systems is essential for maintaining metabolic homeostasis and enabling rapid physiological adaptation[1–6]. Pancreatic islets, highly specialized endocrine micro-organs that tightly regulate blood glucose levels, depend heavily on neural inputs to rapidly and dynamically adjust hormone secretion in response to fluctuating metabolic demands[7–14]. In particular, during acute metabolic emergencies such as hypoglycemia or the fight-or-flight response, timely and synchronized regulation of pancreatic islets by the sympathetic nervous system is crucial for restoring blood glucose levels and thus ensuring survival. However, given their dispersed distribution within the pancreas, how sympathetic nerves coordinate rapid and synchronized control of multiple islets under these critical conditions remains unclear. This suggests a specialized neural-islet architecture supporting such coordinated control — an anatomical relationship conventional two-dimensional histological methods cannot resolve at the whole-organ scale[15–20].

Recently, advances in whole-organ tissue clearing combined with 3D imaging have opened new possibilities to address these critical technical challenges, enabling investigations into islet microstructure, vascular networks, and neural innervation at unprecedented spatial resolution[21–27]. Nevertheless, due to the inherently soft, anatomically complex, and highly convoluted nature of mouse pancreatic tissue, precisely mapping the global 3D structural relationships between islets and neural networks remains technically challenging. Here, we overcame these technical

limitations by fully unfolding the pancreas and employing whole-organ tissue clearing combined with advanced 3D imaging. This enabled us to identify an intimate structural association specifically between sympathetic nerves and pancreatic islets, a relationship notably absent for parasympathetic and sensory nerves.

Building on this newly identified anatomical relationship, we further explored its underlying mechanisms. Developmental studies have previously demonstrated that disruption of sympathetic innervation during early pancreatic development severely impairs islet architecture and profoundly compromises hormone secretion[28,29], reinforcing the classical view of islets as passive recipients of neural inputs whose structural and functional integrity critically depends on innervation. Extending this classical view, our findings provide evidence that the intimate structural relationship between sympathetic nerves and pancreatic islets is actively established and maintained by the islets themselves. These results significantly expand our understanding of endocrine-neural interactions, highlighting an active role for islets in shaping their neural environment.

Results

1. Pancreatic islets are intimately and regularly associated with sympathetic nerves

We first performed a robust method to fully unfold the convoluted mouse pancreas (Extended Data Fig.1a), enabling efficient whole-pancreas tissue clearing (Extended Data Fig.1b). Subsequent advanced 3D imaging provided unprecedented visualization of pancreatic neural networks and their precise spatial relationships with pancreatic islets. To comprehensively characterize the innervation pattern, we specifically labeled sympathetic nerves with tyrosine hydroxylase (TH), parasympathetic nerves with vesicular acetylcholine transporter (VAChT), and sensory nerves with calcitonin gene-related peptide (CGRP). These nerves were labeled in magenta fluorescence, while islets were labeled with insulin (green) and nuclei with DAPI (blue).

Strikingly, sympathetic nerves exhibited a highly organized architecture analogous to "electrical wiring", characterized by a prominent central conduit traversing the pancreas and numerous finer branches extensively distributed throughout the tissue (Fig.1a; Supplementary Video 1). Pancreatic islets were not randomly scattered but precisely positioned along these sympathetic nerve fibers, reminiscent of "light bulbs" systematically arranged along "electrical cords" (Fig.1a-d). High-resolution imaging confirmed intimate spatial contacts between sympathetic fibers and pancreatic islets (Fig.1e), clearly illustrated by 3D reconstructions (Fig.1f, g). This anatomical organization might function similarly to "electrical wiring" powering synchronized

106 illumination of connected “bulbs”, enabling islets to simultaneously respond to
107 sympathetic signals. We also examined parasympathetic and sensory innervation in
108 relation to pancreatic islets but did not observe the structured “wiring-light bulb”-like
109 arrangement seen with sympathetic nerves (Extended Data Fig.2; Supplementary
110 Videos 2, 3).
111
112 The unique anatomical arrangement between islets and sympathetic nerves likely
113 supports their coordinated biological functions. However, it remains unclear how this
114 pattern arises — whether determined by the pancreatic environment or actively
115 shaped by islets themselves.
116
117 **2. Islets recruit sympathetic nerves independently of the pancreatic**
118 **environment**
119 To distinguish between these two possibilities, we isolated approximately 500 islets
120 from healthy 8-week-old mice and transplanted them beneath the renal capsule of
121 streptozotocin (STZ)-induced diabetic mice[30,31], establishing a heterotopic
122 transplantation model (Fig.2a). Using this system, we rigorously tested whether islets
123 could intrinsically establish similar spatial relationships with sympathetic nerves
124 independent of their native pancreatic environment. Post-transplantation monitoring
125 confirmed graft viability and restored endocrine function, indicated by normalized
126 blood glucose levels (Extended Data Fig.3b, e). Notably, the model employed here

127 was primarily intended to investigate biological mechanisms rather than to serve as a
128 therapeutic approach for diabetes.
129
130 We performed whole-kidney 3D imaging at day 120 post-transplantation, which
131 clearly demonstrated sympathetic innervation of transplanted islets (islets, green;
132 sympathetic nerves, magenta) from both horizontal (0°) and tilted (45°) perspectives
133 (Fig.2b; Supplementary Video 4). At day 120, sympathetic fibers were notably
134 extended toward the transplanted islets (Fig.2b, left; white arrowheads). To capture
135 the dynamics of sympathetic nerve recruitment, we conducted tissue clearing imaging
136 at intermediate time points (days 10, 20, 30, 40, and 50; Extended Data Fig.3a left;
137 Supplementary Videos 5-9). Directional nerve growth toward transplanted islets was
138 evident as early as day 10 and progressively strengthened. Quantitative analysis
139 (Extended Data Fig.3c, d) revealed a significant increase in sympathetic nerve growth
140 and branching at day 50 compared to day 10.
141
142 We performed detailed 3D reconstruction to clearly distinguish newly extended, islet-
143 recruited sympathetic nerves (yellow, indicated by white arrowheads) from pre-
144 existing renal sympathetic nerves (magenta), along with transplanted islets (green)
145 and the adrenal gland (blue) (Fig. 2b, right; Extended Data Fig.3a, right;
146 Supplementary Videos 4-9). Quantitative analysis revealed a progressive increase in
147 sympathetic nerve length and branching toward transplanted islets, reaching
148 significantly elevated levels by 120 days post-transplantation (Fig.2c, d).

149 **3. Islets maintain sympathetic innervation and promote regeneration after**
150 **denervation**

151 Based on our finding that transplanted islets actively recruit sympathetic nerves in an
152 ectopic environment, we next explored whether islets similarly regulate sympathetic
153 innervation within their native pancreatic environment.

154

155 Initially, during experiments involving chronic islet injury induced by STZ, we
156 unexpectedly observed pronounced disruption of pancreatic sympathetic nerves
157 approximately 140 days post-treatment (Fig.3a, right; Supplementary Video 10). In
158 contrast, control mice receiving solvent injections maintained sympathetic nerve
159 architecture (Fig.3a, left; Supplementary Video 11). This finding revealed a
160 previously unrecognized role of islets in maintaining pancreatic sympathetic nerve
161 integrity.

162

163 Subsequently, to determine whether islets exhibit similar nerve-attracting properties
164 within the native pancreas, we selectively ablated sympathetic nerves via
165 intrapancreatic injection of 6-hydroxydopamine (6-OHDA). Successful denervation
166 was confirmed at early time points (Extended Data Fig.4; Supplementary Videos 12-
167 14). As anticipated, time-course analyses (days 47, 56, and 65 post-denervation)
168 revealed progressive regeneration of sympathetic nerves and re-established organized
169 interactions with islets (Fig.3b, upper; Supplementary Videos 15-17). By contrast,
170 severe islet injury induced by STZ administration one day post-denervation markedly

171 impaired nerve regeneration, resulting in sparse, disorganized sympathetic fibers
172 (Fig.3b, lower; Supplementary Videos 18-20). Control mice injected with solvents
173 maintained sympathetic innervation, ruling out nonspecific effects of vehicle
174 injections. (Extended Data Fig.5; Supplementary Videos 21-23).
175
176 These results collectively revealed an essential and previously unrecognized role of
177 pancreatic islets in maintaining sympathetic nerve integrity under physiological
178 conditions and actively promoting nerve regeneration following injury, likely through
179 the secretion of specific molecular factors.
180
181 **4. Sympathetic denervation induces islet-specific upregulation of Reg-family**
182 **proteins, especially Reg2 and Reg3β**
183 To investigate the molecular mechanisms underlying islet-induced sympathetic nerve
184 regeneration, we utilized the in situ sympathetic nerve ablation model induced by 6-
185 OHDA described above. On day 7 post-denervation, pancreatic islets were directly
186 isolated from their native pancreatic environment by laser-capture microdissection
187 (LCM) (Fig.4a). This approach preserved the native state of the islets and avoided
188 potential alterations in their secretory profiles during isolation. Subsequent mRNA
189 sequencing analysis revealed significant changes in gene expression, particularly a
190 marked upregulation of regenerating gene family (Reg-family) members, notably
191 *Reg2* and *Reg3b* (Fig. 4b).
192

193 To further clarify the dynamic expression patterns of Reg-family genes following
194 sympathetic nerve injury, and to obtain sufficient islet samples for analysis at multiple
195 time points, we subsequently utilized conventional islet isolation methods to collect
196 islets at days 3, 7, 14, and 21 post-denervation for additional mRNA sequencing
197 analysis (Fig.4c). Consistent with the LCM-based findings, most Reg-family members,
198 particularly *Reg2 and Reg3b*, exhibited significantly elevated expression levels from
199 day 7 onward (Fig.4d). These findings were independently validated by real-time
200 quantitative PCR (RT-qPCR) analysis, confirming significant upregulation of *Reg2*
201 *and Reg3b* (Fig.4e). Given that Reg-family proteins are well-established secretory
202 factors implicated in tissue repair and regeneration[32–34], our results strongly suggest
203 that islet-derived Reg-family proteins, particularly Reg2 and Reg3β, serve as key
204 molecular cues guiding sympathetic nerve regeneration toward pancreatic islets.
205

206 **5. Exogenous Reg2 and Reg3β accelerate sympathetic nerve growth and enhance**
207 **islet graft function**

208 To functionally validate the importance of Reg2 and Reg3β and explore potential
209 translational implications, we initially transplanted pancreatic islets encapsulated in a
210 hydrogel matrix containing exogenous recombinant Reg2 (rReg2) and Reg3β (rReg3β)
211 beneath the renal capsule of recipient mice. At day 50 post-transplantation, whole-
212 kidney clearing and 3D imaging revealed that local administration of rReg2 and
213 rReg3β significantly enhanced sympathetic nerve regeneration, as evidenced by
214 increased nerve length, branching, and directional growth toward transplanted islets
215 compared with controls (Fig.5a, b; Supplementary Video 24).

216 Given the potential limitations of local protein delivery in clinical contexts, we next
217 assessed the efficacy of a more practical route — intraperitoneal administration of
218 rReg2 and rReg3β — in promoting sympathetic regeneration. Recombinant proteins
219 were administered intraperitoneally (i.p.) on days 1, 3, and 5 post-transplantation.
220 Tissues analyzed 35 days post-transplantation showed that systemic delivery also
221 robustly promoted sympathetic regeneration, with significantly increased nerve length
222 and branching toward transplanted islets (Fig.5c, d; Supplementary Video 25).
223
224 To further confirm that endogenous Reg2 and Reg3β specifically mediate sympathetic
225 nerve regeneration toward islets, we used lentiviral-mediated RNA interference to
226 knock down *Reg2* and *Reg3b* expression in isolated islets prior to transplantation
227 (lentiviral sequences provided in Supplementary Table 1), and knockdown efficiency
228 was confirmed by RT-qPCR analysis (Extended Data Fig.6d). At day 60 post-
229 transplantation, sympathetic regeneration toward islets with *Reg2* and *Reg3b*
230 knockdown was significantly delayed, characterized by reduced nerve length and
231 branching compared to controls (Fig.5e, f; Supplementary Video 26).
232
233 Representative whole-kidney clearing images and corresponding 3D reconstructions
234 (horizontal 0° view, Fig.5a, c, e; titled 45° view, Extended Data Fig.6a-c)
235 comprehensively illustrate the spatial interactions between sympathetic nerves and
236 transplanted islets under these experimental conditions. White arrowheads indicate
237 sympathetic fibers clearly directed toward the transplanted islets.
238 To evaluate whether Reg2 and Reg3β-mediated sympathetic nerve regeneration
239 functionally enhances transplanted islets, we administered combined local and
240 systemic rReg2 and rReg3β treatment during islet transplantation. Subsequently,

241 intraperitoneal glucose tolerance tests (IPGTT) were performed at days 30 and 50
242 post-transplantation. Mice receiving rReg2 and rReg3β-treated islets exhibited
243 significantly improved glucose tolerance compared to controls receiving islets alone.
244 Notably, this functional enhancement was more pronounced at day 50 than at day 30
245 (Fig.5g, h). These results suggest that Reg2 and Reg3β not only accelerate but also
246 support prolonged functional performance of transplanted islets, highlighting the
247 therapeutic promise of Reg proteins for enhancing clinical outcomes in islet
248 transplantation and managing diabetes more effectively (Supplementary Video 27).
249

250 **Discussion**

251 Pancreatic islets, essential regulators of glucose homeostasis, are dispersed micro-
252 organs within the pancreas[35,36]. This unique distribution enables islets to precisely
253 monitor and rapidly respond to glucose fluctuations, yet raises a fundamental
254 physiological question: how do dispersed islets achieve synchronized neural
255 integration during acute metabolic stress, such as severe hypoglycemia or fight-or-
256 flight responses[37–39]? Here, we reveal for the first time a precise, "wiring-light bulb"
257 anatomical arrangement, where islets ("light bulbs") align closely along fine
258 sympathetic nerve branches ("wiring"). This specialized organization provides a
259 structural foundation for rapid and coordinated neural integration, analogous to
260 multiple bulbs simultaneously illuminating once electrical current passes through the
261 wiring, highlighting how "**structure dictates function"** in neural signaling.
262

263 Using renal subcapsular transplantation, we confirmed that pancreatic islets actively
264 shape their specialized sympathetic innervation independently of the pancreatic
265 environment, and similarly promote sympathetic nerve regeneration following injury
266 within the native pancreas. Notably, chronic islet injury resulted in progressive
267 disruption of pancreatic sympathetic networks, further uncovering a previously
268 unrecognized role of islets in actively maintaining sympathetic neural integrity. These
269 findings collectively extend the classical view of endocrine organs beyond passive
270 neural targets[40,41], revealing instead their active participation in both establishing and
271 preserving neural architecture. This introduces a novel biological paradigm for organ-
272 nerve interactions: **function shapes and sustains structure**, a principle potentially
273 applicable to other endocrine organs.
274
275 Here, we identified Reg-family proteins, particularly Reg2 and Reg3β, as critical
276 mediators enhancing both islet graft function and sympathetic nerve regeneration,
277 with therapeutic efficacy notably increasing over time. Traditionally associated with
278 inflammation[42,43], tissue repair[44], and regeneration[34,45], Reg proteins had not
279 previously been studied in a neuro-endocrine context. Our findings substantially
280 expand the functional repertoire of these proteins, uncovering their novel capacity to
281 directly facilitate sympathetic nerve growth and promote the functional maturation of
282 transplanted islets. This dual role positions Reg2 and Reg3β as promising therapeutic
283 candidates not only for improving clinical outcomes in islet transplantation but also
284 for preserving sympathetic nerve integrity compromised during diabetes progression.

285 Further exploration of their translational potential could provide innovative strategies
286 for managing metabolic and neural complications associated with diabetes.
287
288 Despite these advances, key questions remain unanswered. First, it remains unclear
289 whether the specialized anatomical arrangement between sympathetic nerves and
290 pancreatic islets observed in mice is conserved in humans. Second, although we
291 identified Reg2 and Reg3β as critical mediators of sympathetic nerve regeneration,
292 their specific cellular sources, molecular mechanisms, and signaling pathways within
293 islets require further elucidation. Future studies using human islets or organoids
294 combined with single-cell RNA sequencing and spatial transcriptomics could address
295 these gaps. Finally, optimal delivery methods, precise dosage, and combinations with
296 other neurotrophic factors must be defined to facilitate clinical translation.
297
298 In summary, our findings redefine the fundamental relationship between endocrine
299 organs and neural networks, uncovering a previously unrecognized biological
300 principle whereby pancreatic islets actively construct and sustain their specialized
301 sympathetic architecture. This reveals an innovative paradigm in neuro-endocrine
302 biology: endocrine organs are not passively regulated by neural inputs but instead
303 actively shape and maintain neural circuits to optimize physiological outcomes. By
304 identifying Reg2 and Reg3β as critical molecular orchestrators, we open avenues for
305 novel therapeutic strategies not only for diabetes but potentially for broader metabolic
306 and neurological disorders where neural integrity is compromised. Future research

307 should explore whether similar organ-driven neural remodeling occurs across other
308 endocrine systems, providing generalizable insights into organ-nerve interactions and
309 expanding therapeutic possibilities for metabolic and neurological disorders.
310

311 **References: Manuscripts**

312 1. Thorens, B. (2010). Central control of glucose homeostasis: the brain – endocrine
313 pancreas axis. Diabetes. Metab. *36*, S45–S49. https://doi.org/10.1016/S1262-
314 3636(10)70466-3.

315 2. Faber, C.L., Deem, J.D., Campos, C.A., Taborsky, G.J., and Morton, G.J. (2020).
316 CNS control of the endocrine pancreas. Diabetologia *63*, 2086–2094.
317 https://doi.org/10.1007/s00125-020-05204-6.

318 3. Hyun, U., and Sohn, J.-W. (2022). Autonomic control of energy balance and
319 glucose homeostasis. Exp. Mol. Med. *54*, 370–376.
320 https://doi.org/10.1038/s12276-021-00705-9.

321 4. Jimenez-Gonzalez, M., Li, R., Pomeranz, L.E., Alvarsson, A., Marongiu, R.,
322 Hampton, R.F., Kaplitt, M.G., Vasavada, R.C., Schwartz, G.J., and Stanley, S.A.
323 (2022). Mapping and targeted viral activation of pancreatic nerves in mice reveal
324 their roles in the regulation of glucose metabolism. Nat. Biomed. Eng. *6*, 1298–
325 1316. https://doi.org/10.1038/s41551-022-00909-y.

326 5. Martinez-Sanchez, N., Sweeney, O., Sidarta-Oliveira, D., Caron, A., Stanley, S.A.,
327 and Domingos, A.I. (2022). The sympathetic nervous system in the 21st century:

328 Neuroimmune interactions in metabolic homeostasis and obesity. Neuron *110*,
329 3597–3626. https://doi.org/10.1016/j.neuron.2022.10.017.

330 6. Agerskov, R.H., and Nyeng, P. (2024). Innervation of the pancreas in
331 development and disease. Development *151*, dev202254.
332 https://doi.org/10.1242/dev.202254.

333 7. Ahrén, B., Ericson, L.E., Lundquist, I., Lorén, I., and Sundler, F. (1981).
334 Adrenergic innervation of pancreatic islets and modulation of insulin secretion by
335 the sympatho-adrenal system. Cell. Tissue. Res. *216*, 15–30.
336 https://doi.org/10.1007/BF00234541.

337 8. Ahrén, B. (2000). Autonomic regulation of islet hormone secretion –
338 Implications for health and disease. Diabetologia *43*, 393–410.
339 https://doi.org/10.1007/s001250051322.

340 9. Rodriguez-Diaz, R., Speier, S., Molano, R.D., Formoso, A., Gans, I., Abdulreda,
341 M.H., Cabrera, O., Molina, J., Fachado, A., Ricordi, C., et al. (2012). Noninvasive
342 in vivo model demonstrating the effects of autonomic innervation on pancreatic
343 islet function. Proc. Natl. Acad. Sci. U.S.A. *109*, 21456–21461.
344 https://doi.org/10.1073/pnas.1211659110.

345 10. Rodriguez-Diaz, R., and Caicedo, A. (2014). Neural control of the endocrine
346 pancreas. Best Pract. Res. Clin. Endocrinol. Metab. *28*, 745–756.
347 https://doi.org/10.1016/j.beem.2014.05.002.

348 11. Proshchina, A.E., Krivova, Y.S., Barabanov, V.M., and Saveliev, S.V. (2014).
349 Ontogeny of neuro-insular complexes and islets innervation in the human
350 pancreas. Front. Endocrinol. (Lausanne) *5*, 57.
351 https://doi.org/10.3389/fendo.2014.00057.

352 12. Li, W., Yu, G., Liu, Y., and Sha, L. (2019). Intrapancreatic Ganglia and Neural
353 Regulation of Pancreatic Endocrine Secretion. Front. Neurosci. *13*.
354 https://doi.org/10.3389/fnins.2019.00021.

355 13. Lin, E.E., Scott-Solomon, E., and Kuruvilla, R. (2021). Peripheral Innervation in
356 the Regulation of Glucose Homeostasis. Trends. Neurosci. *44*, 189–202.
357 https://doi.org/10.1016/j.tins.2020.10.015.

358 14. Papazoglou, I., Lee, J.-H., Cui, Z., Li, C., Fulgenzi, G., Bahn, Y.J., Staniszewska-
359 Goraczniak, H.M., Piñol, R.A., Hogue, I.B., Enquist, L.W., et al. (2022). A
360 distinct hypothalamus-to-β-cell circuit modulates insulin secretion. Cell Metab. *34*,
361 285-298.e7. https://doi.org/10.1016/j.cmet.2021.12.020.

362 15. Cabrera-Vásquez, S., Navarro-Tableros, V., Sánchez-Soto, C., Gutiérrez-Ospina,
363 G., and Hiriart, M. (2009). Remodelling sympathetic innervation in rat pancreatic
364 islets ontogeny. BMC. Dev. Biol. *9*, 34. https://doi.org/10.1186/1471-213X-9-34.

365 16. Rodriguez-Diaz, R., and Caicedo, A. (2013). Novel approaches to study the role
366 innervation plays in the biology of pancreatic islets. Endocrinol. Metab. Clin.
367 North Am. *42*, 39–56. https://doi.org/10.1016/j.ecl.2012.11.001.

368 17. Campbell-Thompson, M., Butterworth, E.A., Boatwright, J.L., Nair, M.A., Nasif,
369 L.H., Nasif, K., Revell, A.Y., Riva, A., Mathews, C.E., Gerling, I.C., et al. (2021).
370 Islet sympathetic innervation and islet neuropathology in patients with type 1
371 diabetes. Sci. Rep. *11*, 6562. https://doi.org/10.1038/s41598-021-85659-8.

372 18. Lkhagvasuren, B., Mee-inta, O., Zhao, Z.-W., Hiramoto, T., Boldbaatar, D., and
373 Kuo, Y.-M. (2021). Pancreas-Brain Crosstalk. Front. Neuroanat. *15*, 691777.
374 https://doi.org/10.3389/fnana.2021.691777.

375 19. Makhmutova, M., and Caicedo, A. (2021). Optical Imaging of Pancreatic
376 Innervation. Front. Endocrinol. (Lausanne) *12*, 663022.
377 https://doi.org/10.3389/fendo.2021.663022.

378 20. Krivova, Y.S., Proshchina, A.E., Otlyga, D.A., Leonova, O.G., and Saveliev, S.V.
379 (2022). Prenatal development of sympathetic innervation of the human pancreas.
380 Ann. Anat.-Anat. Anz *240*, 151880. https://doi.org/10.1016/j.aanat.2021.151880.

381 21. Tseng, S.-J., Lee, Y.-H., Chen, Z.-H., Lin, H.-H., Lin, C.-Y., and Tang, S.-C.
382 (2009). Integration of optical clearing and optical sectioning microscopy for
383 three-dimensional imaging of natural biomaterial scaffolds in thin sections. J.
384 Biomed. Opt. *14*, 044004. https://doi.org/10.1117/1.3158998.

385 22. Fu, Y.-Y., Lu, C.-H., Lin, C.-W., Juang, J.-H., Enikolopov, G., Sibley, E., Chiang,
386 A.-S., and Tang, S.-C. (2010). Three-dimensional optical method for integrated
387 visualization of mouse islet microstructure and vascular network with subcellular-

388 level resolution. J. Biomed. Opt. *15*, 046018. https://doi.org/10.1117/1.3470241.

389 23. Chiu, Y.-C., Hua, T.-E., Fu, Y.-Y., Pasricha, P.J., and Tang, S.-C. (2012). 3-D
390 imaging and illustration of the perfusive mouse islet sympathetic innervation and
391 its remodelling in injury. Diabetologia *55*, 3252–3261.
392 https://doi.org/10.1007/s00125-012-2699-6.

393 24. Tang, S.-C., Peng, S.-J., and Chien, H.-J. (2014). Imaging of the islet neural
394 network. Diabetes. Obes. Metab. *16*, 77–86. https://doi.org/10.1111/dom.12342.

395 25. Yang, Y.H.C., Kawakami, K., and Stainier, D.Y. (2018). A new mode of
396 pancreatic islet innervation revealed by live imaging in zebrafish. eLife *7*, e34519.
397 https://doi.org/10.7554/eLife.34519.

398 26. Alvarsson, A., Jimenez-Gonzalez, M., Li, R., Rosselot, C., Tzavaras, N., Wu, Z.,
399 Stewart, A.F., Garcia-Ocaña, A., and Stanley, S.A. (2020). A 3D atlas of the
400 dynamic and regional variation of pancreatic innervation in diabetes. Sci. Adv. *6*,
401 eaaz9124. https://doi.org/10.1126/sciadv.aaz9124.

402 27. Alvarsson, A., Jimenez-Gonzalez, M., Li, R., Rosselot, C., Tzavaras, N., Wu, Z.,
403 and Stanley, S.A. (2021). Optical Clearing and 3D Analysis Optimized for Mouse
404 and Human Pancreata. Bio-protocol *11*, e4103.
405 https://doi.org/10.21769/BioProtoc.4103.

406 28. Borden, P., Houtz, J., Leach, S.D., and Kuruvilla, R. (2013). Sympathetic
407 Innervation during Development Is Necessary for Pancreatic Islet Architecture

408 and Functional Maturation. Cell Rep. *4*, 287–301.
409 https://doi.org/10.1016/j.celrep.2013.06.019.

410 29. Scott-Solomon, E., Boehm, E., and Kuruvilla, R. (2021). The sympathetic
411 nervous system in development and disease. Nat. Rev. Neurosci. *22*, 685–702.
412 https://doi.org/10.1038/s41583-021-00523-y.

413 30. Szot, G.L., Koudria, P., and Bluestone, J.A. (2007). Transplantation of Pancreatic
414 Islets Into the Kidney Capsule of Diabetic Mice. J. Vis. Exp. *9*, 404.
415 https://doi.org/10.3791/404.

416 31. Li, D., Kong, W., Hong, Y., Zhang, W., Sun, B., Wang, X., and Wang, K. (2025).
417 Protocol for isolation and transplantation of rat pancreatic islets in the kidney
418 capsule to treat diabetes. Star. Protoc. *6*, 103486.
419 https://doi.org/10.1016/j.xpro.2024.103486.

420 32. Okamoto, H. (1999). The Reg gene family and Reg proteins: with special
421 attention to the regeneration of pancreatic beta-cells. J. Hepatobiliary. Pancreat.
422 Surg. *6*, 254–262. https://doi.org/10.1007/s005340050115.

423 33. Wu, H., Zheng, Q., Rengabhashyam, P., and Zenilman, M.E. (2000). A Brief
424 History of Pancreatic Reg: Implications as to its Clinical Importance. Einstein Q.
425 J. Biol. Med. *17*, 178.

426 34. Namikawa, K., Fukushima, M., Murakami, K., Suzuki, A., Takasawa, S.,
427 Okamoto, H., and Kiyama, H. (2005). Expression of Reg/PAP family members

428 during motor nerve regeneration in rat. Biochem. Biophys. Res. Commun. *332*,
429 126–134. https://doi.org/10.1016/j.bbrc.2005.04.105.

430 35. Röder, P.V., Wu, B., Liu, Y., and Han, W. (2016). Pancreatic regulation of
431 glucose homeostasis. Exp. Mol. Med. *48*, e219.
432 https://doi.org/10.1038/emm.2016.6.

433 36. Abdulreda, M.H., and Berggren, P.O. (2021). The pancreatic islet: a micro-organ
434 in control. CellR4 *9*, e3093. https://doi.org/10.32113/cellr4_20213_3093.

435 37. Morton, G.J., Muta, K., Kaiyala, K.J., Rojas, J.M., Scarlett, J.M., Matsen, M.E.,
436 Nelson, J.T., Acharya, N.K., Piccinini, F., Stefanovski, D., et al. (2017). Evidence
437 That the Sympathetic Nervous System Elicits Rapid, Coordinated, and Reciprocal
438 Adjustments of Insulin Secretion and Insulin Sensitivity During Cold Exposure.
439 Diabetes *66*, 823–834. https://doi.org/10.2337/db16-1351.

440 38. Noguchi, G.M., and Huising, M.O. (2019). Integrating the inputs that shape
441 pancreatic islet hormone release. Nat. Metab. *1*, 1189–1201.
442 https://doi.org/10.1038/s42255-019-0148-2.

443 39. De Rosa, M.J., Veuthey, T., Florman, J., Grant, J., Blanco, M.G., Andersen, N.,
444 Donnelly, J., Rayes, D., and Alkema, M.J. (2019). The flight response impairs
445 cytoprotective mechanisms by activating the insulin pathway. Nature *573*, 135–
446 138. https://doi.org/10.1038/s41586-019-1524-5.

447 40. Hampton, R.F., Jimenez-Gonzalez, M., and Stanley, S.A. (2022). Unravelling

448 innervation of pancreatic islets. Diabetologia *65*, 1069–1084.
449 https://doi.org/10.1007/s00125-022-05691-9.

450 41. Ulrich-Lai, Y.M., and Herman, J.P. (2009). Neural regulation of endocrine and
451 autonomic stress responses. Nat. Rev. Neurosci. *10*, 397–409.
452 https://doi.org/10.1038/nrn2647.

453 42. Sun, C., Wang, X., Hui, Y., Fukui, H., Wang, B., and Miwa, H. (2021). The
454 Potential Role of REG Family Proteins in Inflammatory and Inflammation-
455 Associated Diseases of the Gastrointestinal Tract. Int. J. Mol. Sci. *22*, 7196.
456 https://doi.org/10.3390/ijms22137196.

457 43. Chen, W., Imasaka, M., Lee, M., Fukui, H., Nishiura, H., and Ohmuraya, M.
458 (2023). Reg family proteins contribute to inflammation and pancreatic stellate
459 cells activation in chronic pancreatitis. Sci. Rep. *13*, 12201.
460 https://doi.org/10.1038/s41598-023-39178-3.

461 44. Yu, L., Wu, Q., Jiang, S., Liu, J., Liu, J., and Chen, G. (2025). Controversial
462 Roles of Regenerating Family Proteins in Tissue Repair and Tumor Development.
463 Biomedicines *13*, 24. https://doi.org/10.3390/biomedicines13010024.

464 45. Okamoto, H. (1999). The Reg gene family and Reg proteins: with special
465 attention to the regeneration of pancreatic β-cells. J. Hep. Bil. Pancr. Surg. *6*,
466 254–262. https://doi.org/10.1007/s005340050115.

467

468

469 **Methods**

470 **Ethical approval**

471 All animal experiments conducted in this study were approved by the Institutional
472 Animal Ethics Committee of the Shanghai Cancer Institute (A2024170-004), Ren Ji
473 Hospital, School of Medicine, Shanghai Jiao Tong University. Experiments were
474 performed strictly in accordance with institutional guidelines and ethical standards.

475

476 **Animals**

477 Male C57BL/6J mice (8-10 weeks old) were obtained from Vitalriver and maintained
478 under specific pathogen-free conditions (temperature: 22 ± 2 °C; humidity: 55% ± 5%;
479 12-h light/dark cycle) at Shanghai Jiao Tong University, with ad libitum access to
480 standard rodent chow and water. Body weight, food intake, and water consumption
481 were recorded regularly. All animal procedures were approved by the Institutional
482 Animal Care and Use Committee (IACUC) of Shanghai Jiao Tong University and
483 followed the NIH Guide for the Care and Use of Laboratory Animals.

484

485 **Whole-organ clearing and labeling**

486 ***Tissue harvesting***

487 Mice were deeply anesthetized via intraperitoneal (i.p.) injection of sodium
488 pentobarbital (50 mg/kg, RWD, r510-22) and perfused transcardially with phosphate-
489 buffered saline (PBS, Servicebio, G4202) followed by 4% paraformaldehyde (PFA,
490 Servicebio, G1101). The pancreas was carefully dissected, rinsed in PBS, and placed

491 on a moist filter paper. To preserve the organ's spatial architecture, the pancreas was
492 gently spread out and pinned at the edges using fine needles (Extended Data Fig.1a).

493 ***3D immunolabeling***

494 The sample was treated with methanol solutions for 3 days at room temperature and
495 bleached with a 5% H_2O_2 solution overnight at 4°C. Then, the sample was treated
496 with 0.2% Triton X-100 solution for 3 days at room temperature with shaking.
497 Subsequently, the sample was immersed in a 10% donkey serum blocking solution for
498 3 days at room temperature, followed by incubation in the primary antibody solution
499 (TH, 1:500, rabbit, ab112, Abcam; Insulin, 1:500, rat, MAB1417, R&D Systems) for
500 6 days at room temperature, and then in the secondary antibody solution (donkey anti-
501 rabbit 561 nm, 1:500, A32794, Invitrogen; donkey anti-rat 488 nm, 1:500, A21208,
502 Invitrogen; DAPI, 1:500, D1306, Invitrogen) for 6 days at room temperature. After
503 immersion in the antibody solutions, the sample was washed with 0.2% Tween-20
504 solution for 2 days at room temperature[46]. Detailed antibody information is
505 summarized in Table 1.

506 ***Clearing method***

507 The FDISCO (fluorescence imaging of solvent-cleared organs with superior
508 fluorescence-preserving capability) tissue clearing reagent kit (JA11012, Jarvisbio)
509 was used in this study[47]. The clearing procedure was performed strictly according to
510 the manufacturer's instructions. Briefly, labeled mouse pancreas samples were
511 sequentially incubated in reagents A, B, C, and D for 6 hours each, followed by

512 reagent E for 12 hours, and finally incubated in reagent F until complete transparency
513 was achieved. All incubations were conducted at 6-8 °C with gentle shaking.
514

515 **3D fluorescence imaging and digital reconstruction of cleared tissues**

516 ***Light-sheet microscope***

517 The cleared samples were imaged using a light sheet microscope (LiToneXL, Light
518 Innovation Technology) equipped with a 4× objective lens (NA = 0.28, working
519 distance = 20 mm). Thin light sheets were illuminated from the four sides of samples,
520 and a merged image was saved. To acquire images, the cleared samples were
521 manually attached to the sample holder adapter. Subsequently, the samples were
522 immersed in imaging reagent within a 3D printing sample chamber and excited with
523 light sheets of different wavelengths.

524 ***Confocal microscope***

525 The cleared tissue samples were mounted on two cover glasses and imaged using an
526 inverted confocal fluorescence microscope (LSM880, Zeiss, Germany) equipped with
527 the Plan Apochromat 10×/0.45 objective (dry lens; working distance = 2.0 mm), Plan
528 Apochromat 20×/0.8 objective (dry lens; working distance = 0.55 mm), and Plan
529 Apochromat 40×/0.95 objective (water immersion lens; working distance = 0.20 mm).
530 The collected images were subsequently processed with Zen software (Zeiss,
531 Germany) and reconstructed into 3D images using Imaris software (Version 7.2.3,
532 Bitplane, Switzerland)[48].

533 ***Imaging data processing***

534 The resulting TIFF raw data images were stitched and converted using LitScan
535 software and subsequently analyzed with Imaris software[48].

536 ***Digital reconstruction and quantitative analysis of cleared nerve fibers***

537 The Filament module of Imaris software was used for 3D tracing of nerve fibers in
538 cleared tissues. Cone mode and AutoDepth mode were selected to accurately locate
539 and delineate the nerve fibers, and the segment diameters were adjusted according to
540 the actual diameters of nerve trunks and branches. Finally, filament length and
541 branching points were quantified using the statistics panel of the Filament module.

542

543 **Islet isolation and renal subcapsular transplantation**

544 Pancreatic islets were isolated from donor mice using collagenase P (Roche, CollP-
545 RO) digestion and density gradient centrifugation as previously described[49].
546 Approximately 500 islets were evenly divided into two parts and transplanted under
547 the bilateral renal capsule of STZ-induced diabetic recipient mice. For transplantation,
548 mice were anesthetized, and a small incision was made to expose the kidney. Islets
549 were transferred using a Hamilton syringe and gently injected under the renal capsule.
550 The incision was closed with surgical sutures, and mice were allowed to recover with
551 appropriate postoperative care.

552

553 **Establishment of diabetic mice models**

554 Two distinct protocols for streptozotocin (STZ)-induced diabetes were employed,
555 depending on the experimental purpose. Specifically, a multiple low-dose STZ

556 protocol was used to establish stable diabetes for subsequent islet transplantation
557 experiments. A single high-dose STZ injection was administered one day after
558 sympathetic nerve ablation using 6-hydroxydopamine (6-OHDA) to rapidly induce
559 severe β-cell injury, thus preventing potential confounding effects of residual
560 functional islets on sympathetic nerve regeneration.

561 ***Multiple low-dose STZ induction***

562 Diabetes was induced by daily i.p. injections of STZ (50 mg/kg) dissolved in 0.1 M
563 citrate buffer (pH 4.2-4.5), administered over five consecutive days[50].

564 ***Single high-dose STZ induction following 6-OHDA treatment***

565 Diabetes was induced by a single high-dose i.p. injection of STZ (150 mg/kg), also
566 dissolved in 0.1 M citrate buffer (pH 4.2-4.5)[51]. The injection was given following an
567 8-hour fasting period, specifically one day after pancreatic sympathetic nerve ablation
568 using 6-OHDA.

569 Blood glucose levels were monitored every other day using a glucometer (Accu-Chek,
570 Roche). Mice were defined as diabetic when blood glucose exceeded 16.7 mmol/L in
571 three consecutive measurements.

572

573 **Blood glucose measurement and IPGTT**

574 Random blood glucose levels were measured from tail vein blood using a glucometer.
575 IPGTT were performed after an 8-hour fasting. Mice received an i.p. injection of
576 glucose (2 g/kg), and blood glucose levels were measured at 0, 15, 30, 60, and 120
577 min post-injection[52].

578 **Sympathetic nerve ablation**

579 10-week-old mice were randomly assigned into the vehicle group and the 6-OHDA
580 group. After anesthetizing the mice with isoflurane, the hair in the abdomen was
581 removed and the area was disinfected with povidone-iodine. Then, a small incision
582 was made along the midline of the abdomen skin to expose the pancreas. The
583 pancreas was pulled out gently and fully exposed with sterile tweezers. 6-OHDA
584 (HY-B1081, MCE) was administered by intrapancreatic injection (1 mg in 15 μL
585 saline containing 0.1% L-ascorbic acid [HY-B0166, MCE], 100 mg/kg). To
586 pharmacologically ablate sympathetic nerve in the whole pancreas, this 15-μL dose of
587 6-OHDA was evenly administered from the pancreas head to the tail. Control mice
588 received a 15-μL dose of 0.1% L-ascorbic acid injections.

589

590 **Regenerating protein family (Reg-family) protein administration**

591 Recipient mice were randomly divided into four experimental groups:

592 ***Local administration***

593 Recombinant Reg2 (rReg2) and recombinant Reg3β (rReg3β) proteins (500 nM final
594 concentration) were incorporated into a biocompatible hydrogel matrix (Corning,
595 Cat#354236) at a final concentration of 2 mg/mL. Isolated islets were gently mixed
596 with the Reg-loaded hydrogel. Controls received islets embedded in hydrogel without
597 Reg proteins.

598 ***Systemic administration***

599 Mice received purified islets embedded in a hydrogel matrix (2 mg/mL, Corning,

600 Cat#354236). For the systemic administration group, mice additionally received i.p.
601 injections of rReg2 and rReg3β protein mixture (150 mg/kg, dissolved in sterile
602 ddH_2O at 100 mg/mL) on days 1, 3, and 5 post-transplantation[53,54], starting on the
603 transplantation day. Controls received equal volumes of sterile ddH_2O on the same
604 schedule.
605 All animal procedures were performed under general anesthesia, following
606 institutional animal care and use guidelines.
607

608 **Lentiviral-mediated knockdown of *Reg2* and *Reg3b* expression in pancreatic**
609 **islets**

610 ***shRNA design and vector construction***

611 Three independent shRNA sequences targeting mouse *Reg2* (NCBI Gene ID:
612 NM_009043.2) and *Reg3b* (NCBI Gene ID: NM_011036.1), along with a scrambled
613 control shRNA, were designed and synthesized **(Supplementary Table 2)**. Each
614 sequence was cloned into the lentiviral vector pSLenti-U6-shRNA-CMV-EGFP-F2A-
615 Puro-WPRE.

616 ***Validation of shRNA knockdown efficiency in isolated islets***

617 Freshly isolated mouse pancreatic islets (approximately 100 islet equivalents, IEQ)
618 were pre-cultured overnight in RPMI-1640 medium supplemented with 10% fetal
619 bovine serum (FBS). Equal volumes of lentiviral preparations containing three
620 distinct shRNAs targeting either *Reg2* or *Reg3b* were pre-mixed at a 1:1:1 ratio,
621 ensuring equal multiplicity of infection (MOI) distribution for each shRNA construct.

622 The pooled lentiviral mixtures were added to the pre-cultured islet at a total MOI of
623 10-20 in the presence of polybrene (10 μg/mL). After incubation at 37°C for 8 h, the
624 virus-containing medium was replaced with fresh culture medium. Gene knockdown
625 efficiency was confirmed by RT-qPCR analysis prior to islet transplantation (see
626 Extended Data Fig.7).

627 ***Lentiviral-mediated shRNA delivery during islet transplantation***

628 To achieve efficient *Reg2* and *Reg3b* knockdown during islet transplantation, freshly
629 isolated pancreatic islets were mixed with lentiviral preparations (containing the same
630 shRNA mixture described above) and rapidly encapsulated in a hydrogel matrix. The
631 islet-lentivirus-hydrogel mixture was then incubated for approximately 30 min at
632 37°C to allow complete gelation, and subsequently transplanted beneath the renal
633 capsule of anesthetized recipient mice.

634

635 **Real-time quantitative PCR （RT-qPCR）**

636 Total RNA was extracted from tissues or cells using TRIzol reagent (Invitrogen).
637 cDNA was synthesized using the PrimeScript RT reagent Kit (Takara). RT-qPCR was
638 performed with SYBR Green PCR Master Mix (Applied Biosystems) on a
639 QuantStudio 6 Flex Real-Time PCR System (Applied Biosystems). Gene expression
640 levels were normalized to β-actin and calculated using the $2^{-\Delta\Delta Ct}$ method. Primer
641 sequences are listed in Supplementary Table 3.

642

643 **Transcriptome sequencing of laser-captured pancreatic islets**

644 ***Sample preparing***

645 Formalin-fixed, paraffin-embedded (FFPE) pancreatic tissue was sectioned at 7 μm
646 thickness. Slides were first deparaffinized in xylene for 5 min, rehydrated sequentially
647 through graded ethanol solutions (100%, 95%, 70%, and 50%; 2 min each), and
648 rinsed briefly in distilled water. Sections were then rapidly stained with hematoxylin
649 and eosin (H&E) using an optimized protocol designed to preserve RNA integrity.
650 Following staining, slides were dehydrated in ascending ethanol concentrations,
651 cleared with xylene, and allowed to air-dry completely under RNase-free conditions
652 before further processing.

653 ***Laser-capture microdissection (LCM) and libraries preparation***

654 LCM was performed using a PALM MicroBeam system (Zeiss MicroImaging,
655 Munich, Germany). Islet regions were identified based on morphological criteria
656 under microscopic observation. Approximately 300 islets per sample were precisely
657 isolated via laser microdissection and collected into 200 μL adhesive-capped tubes
658 (Carl Zeiss, cat.no. 415190-9191-000, Jena, Germany). Immediately following
659 collection, 10 μL of LCM lysis mix buffer was added, and tubes were sealed tightly
660 with Parafilm.

661 Transcriptome libraries were generated following the Smart-3SEQ protocol. Briefly,
662 cell lysis and RNA fragmentation were performed at 60°C for 60 min, followed by the
663 addition of 10 μL LCM TS-RT mix for reverse transcription. Amplification of the
664 resulting cDNA and subsequent cleanup were performed according to the published
665 protocol. The final library concentration was measured using a Qubit 3.0 fluorometer

666 (Thermo Fisher Scientific, MA, USA)[55,56].

667 ***Next-generation sequencing***

668 The cDNA libraries were profiled for size distribution on an Agilent 2100 with High
669 Sensitivity D1000 reagent kit (Agilent, Santa Clara, USA) and then stored at -20°C
670 until sequencing. The libraries were sequenced using the Illumina high-throughput
671 sequencing platform NovaSeq 6000 system (Illumina, San Diego, USA) with 2×150
672 bp pair-end mode.

673 ***Data analysis***

674 The FASTQ data were analyzed according to the Smart-3SEQ protocol. Briefly, base
675 calls from the NovaSeq were demultiplexed and converted to FASTQ format and
676 adapter trimming were performed. The first 5nt of each read were removed from its
677 sequence and appended to the read name as its UMI; the following 3nt were assumed
678 to derive from the G-overhand of the template-switch oligonucleotide and were
679 discarded. Reads were aligned by STAR to the mouse reference genome mm10. PCR
680 duplicate reads that start at the same genome position with the same UMI sequence
681 were detected and discarded. Then the transcript abundance was quantified.
682 Differential gene expression was analyzed with DESeq2. The regularized log
683 transformation was used to normalize read counts. PCA was performed on the
684 normalized data with the prcomp function.

685

686 **Bulk RNA-seq of isolated pancreatic islets**

687 Pancreatic islets were isolated from 0.1% L-ascorbic acid or 6-OHDA treated mice

688 using collagenase P (Roche, CollP-RO) digestion and density gradient centrifugation
689 as previously described. Total RNA was extracted from islet samples with the
690 Universal RNA Extraction CZ Kit (RNC643, ONREW) according to the
691 manufacturer's instructions. RNA quantity was analysed using Qubit 4.0 (Invitrogen)
692 and quality examined by electrophoresis on a denaturing agarose gel. RNA libraries
693 were prepared using the VVAHTS® Universal V8 RNA-seq Library Prep Kit for
694 Illumina (NR605-0, Vazyme), followed sequencing using the Illumina NovaSeq 6000
695 platform with the 150 paired-end sequencing strategy. Enrichment of mRNA, library
696 construction, sequencing and data analysis were performed by Shanghai Xu Ran
697 Biotechnology Co., Ltd. The raw data was handled by Skewer v0.2.2
698 (https://sourceforge.net/projects/skewer/files/?source=navbar) and data quality was
699 checked by FastQC v0.11.2 (http://
700 www.bioinformatics.babraham.ac.uk/projects/fastqc/). The read length was 2×150 bp.
701 Clean reads were aligned to the mouse genome GRCm39 (mm10) from ensembl using
702 STAR (https://github.com/alexdobin/STAR), with one mismatch allowed. StringTie
703 (v1.3.1c) was used to generate gene expression data and differential gene expression
704 was analysed by DESeq2 (v1.16.1)
705 (https://bioconductor.org/packages/release/bioc/html/DESeq2.html). The thresholds
706 for determining DEGs are $P < 0.05$ and absolute fold change ≥ 2. Then DEGs were
707 chosen for function and signaling pathway enrichment analysis using TopGO
708 (https://www.bioconductor.org/packages/release/bioc/html/topGO.html) and KEGG
709 database (https://www.genome.jp/kegg/pathway.html). The significantly enriched

710 pathways were determined when $P < 0.05$.

711

712 ***Data availability***

713 The raw sequencing data from the laser capture microdissected samples and the
714 isolated islet samples have been deposited in the NCBI SRA under accession number
715 PRJNA1241420 and PRJNA1243594 respectively. All other data in this article are
716 available from the corresponding author on reasonable request. The datasets generated
717 and analyzed during this study are available via Figshare
718 (https://figshare.com/s/37e36235c0efd54a05a7).

719

720 **References: Methods**

721 46. Nicolas Renier, Adams, E.L., Kirst, C., Wu, Z., Azevedo, R., Kohl, J., Autry,
722 A.E., Kadiri, L., Venkataraju, K.U., Zhou, Y., et al. (2016). Mapping of Brain
723 Activity by Automated Volume Analysis of Immediate Early Genes. Cell *165*, 1789–
724 1802. https://doi.org/10.1016/j.cell.2016.05.007.

725 47. Qi, Y., Yu, T., Xu, J., Wan, P., Ma, Y., Zhu, J., Li, Y., Gong, H., Luo, Q., and
726 Zhu, D. (2019). FDISCO: Advanced solvent-based clearing method for imaging
727 whole organs. Sci. Adv. *5*, eaau8355. https://doi.org/10.1126/sciadv.aau8355.

728 48. Zhu, J., Liu, X., Liu, Z., Deng, Y., Xu, J., Liu, K., Zhang, R., Meng, X., Fei, P.,
729 Yu, T., et al. (2024). SOLID: minimizing tissue distortion for brain-wide profiling of
730 diverse architectures. Nat. Commun. *15*, 8303. https://doi.org/10.1038/s41467-024-
731 52560-7.

732 49. Wang, K., Wang, X., Han, C.-S., Chen, L.-Y., and Luo, Y. (2017). Scaffold-
733 supported Transplantation of Islets in the Epididymal Fat Pad of Diabetic Mice. J. Vis.
734 Exp., 54995. https://doi.org/10.3791/54995.

735 50. Chaudhry, Z.Z., Morris, D.L., Moss, D.R., Sims, E.K., Chiong, Y., Kono, T., and
736 Evans-Molina, C. (2013). Streptozotocin is equally diabetogenic whether
737 administered to fed or fasted mice. Lab. Anim. *47*, 257–265.
738 https://doi.org/10.1177/0023677213489548.

739 51. Chen, H., Liu, J., Shi, G.-P., and Zhang, X. (2023). Protocol for in vivo and
740 ex vivo assessment of hyperglycemia and islet function in diabetic mice. Star. Protoc.
741 *4*, 102133. https://doi.org/10.1016/j.xpro.2023.102133.

742 52. Basco, D., Zhang, Q., Salehi, A., Tarasov, A., Dolci, W., Herrera, P., Spiliotis, I.,
743 Berney, X., Tarussio, D., Rorsman, P., et al. (2018). α-cell glucokinase suppresses
744 glucose-regulated glucagon secretion. Nat. Commun. *9*, 546.
745 https://doi.org/10.1038/s41467-018-03034-0.

746 53. Luo, C., Yu, L.-T., Yang, M.-Q., Li, X., Zhang, Z.-Y., Alfred, M.O., Liu, J.-L.,
747 and Wang, M. (2016). Recombinant Reg3β protein protects against streptozotocin-
748 induced β-cell damage and diabetes. Sci. Rep. *6*, 35640.
749 https://doi.org/10.1038/srep35640.

750 54. Yu, L., Li, X., Zhang, Z., Du, P., Liu, J.-L., Li, Y., Yin, T., Yu, W., Sun, H.,
751 Wang, M., et al. (2019). Dimorphic autoantigenic and protective effects of Reg2
752 peptide in the treatment of diabetic β-cell loss. Diabetes. Obes. Metab. *21*, 1209–1222.

753 https://doi.org/10.1111/dom.13644.

754 55. Zhang, X., Hu, C., Huang, C., Wei, Y., Li, X., Hu, M., Li, H., Wu, J.,
755 Czajkowsky, D.M., Guo, Y., et al. (2022). Robust Acquisition of Spatial
756 Transcriptional Programs in Tissues With Immunofluorescence-Guided Laser Capture
757 Microdissection. Front. Cell. Dev. Biol. *10*, 853188.
758 https://doi.org/10.3389/fcell.2022.853188.

759 56. Wu, Z., Wu, X., Xu, Z., Liu, Y., Zhu, Z., Li, X., Czajkowsky, D.M., Sun, F., Guo,
760 Y., and Shao, Z. (2025). In situ transcriptomic analysis of spermatocytes in non-
761 obstructive azoospermia reveals senescence-like states in arrested spermatocytes.
762 GENES. DIS. *12*, 101205. https://doi.org/10.1016/j.gendis.2024.101205.

763

764 **Acknowledgements**

765 This study was supported by the National Natural Science Foundation of China
766 (92168111, 82230087, 82350123, 82203228), the Shanghai Municipal Education
767 Commission-Gaofeng Clinical Medicine Grant Support (20181708), Innovative
768 research team of high-level local universities in Shanghai (SHSMU-ZDCX20210802),
769 Shanghai Pilot Program for Basic Research - Shanghai Jiao Tong University
770 (21TQ1400225), 111 project (NO. B21024), Shenyang Science and Technology Plan
771 in 2022 (22-101-0-22). We thank Jarvis (Wuhan) Biological Pharmaceutical Co., Ltd.
772 for technical support in tissue clearing and 3D imaging.

773

774 **Author contributions**

775 Z.-G.Z. and D.-X.L. conceived the project and designed experiments. J.-M.L., J.-J.W.,
776 Y.-Z.Q., and D.-X.L. performed experiments and analyzed the data. D.-X.L. and J.-
777 M.L. wrote the manuscript. J.-J.W. and H.-L. performed bioinformatics analyses.
778 D.A., T.Y., Y.-X.H., W.-T.S., X.-Y.M., and M.M. assisted with experiments. L.Z.,
779 X.-M.Y., Y.Q., Y.-L.Z., and Y.-Q.Y. provided technical support. S.-H.J., J.L., L.-P.H.,
780 X.-L.Z., and Q.L. provided critical insights and revised the manuscript. All authors
781 reviewed and approved the final manuscript.
782

783 **Competing interests**

784 The authors declare no competing interests.
785

786 **Figure legends**

787 **Figure 1. Pancreatic islets form a highly organized spatial arrangement along**
788 **sympathetic nerves.**

789 **a**, Whole-pancreas 3D imaging of an unfolded and cleared pancreas from an 8-week-
790 old male mouse (C57BL/6J) reveals a highly organized sympathetic neural network
791 (TH, magenta). Pancreatic islets (insulin, green) are precisely positioned along these
792 sympathetic nerve branches. Nuclei are stained with DAPI (blue). Scale bars: 2500
793 μm. See Supplementary Video 1.

794 **b-d**, Magnified views of representative areas from (a).

795 **e,** High-resolution imaging of a pancreatic islet and sympathetic nerve fibers. Scale
796 bars: 50 μm.

797 **f, g,** 3D reconstructions of the two individual islets shown in (e). Scale bars: 20 μm.

798

799 **Figure 2. Pancreatic islets actively recruit sympathetic nerves independent of the**

800 **pancreatic environment.**

801 **a,** Schematic illustration of the experimental strategy for renal subcapsular

802 transplantation of approximately 500 isolated pancreatic islets into STZ-induced

803 diabetic mice, to evaluate sympathetic nerve recruitment by islets transplanted outside

804 their native pancreatic environment.

805 **b,** Representative whole-kidney clearing images (left) showing sympathetic

806 innervation (TH, magenta), transplanted islets (insulin, green) at day 120 post-

807 transplantation. Corresponding 3D reconstructions (right) illustrate pre-existing

808 sympathetic nerves within the kidney (magenta), islet-recruited sympathetic nerves

809 (yellow), transplanted islets (green), and the adrenal gland (blue), viewed horizontally

810 (0°) and from a tilted angle (45°). White arrowheads indicate sympathetic fibers

811 clearly directed toward the transplanted islets. Sham-operated mice served as controls

812 and exhibited no significant sympathetic nerve recruitment. Scale bars: 1000 μm. See

813 Supplementary Video 4 for dynamic visualization.

814 **c, d,** Quantitative analyses of sympathetic nerve growth recruited by transplanted

815 islets, including total nerve length (c) and branch number (d), assessed at multiple

816 time points (days 10, 20, 30, 40, 50, and 120) post-transplantation. Corresponding

817 whole-tissue clearing and 3D reconstructions for each time point are presented in

818 Supplementary Fig.3 and Supplementary Video 4-9.

819 **Figure 3. Islets maintain pancreatic sympathetic innervation and facilitate**
820 **regeneration following denervation.**
821 **a,** Representative whole-pancreas 3D imaging showing sympathetic nerves (TH,
822 magenta), pancreatic islets (insulin, green), and nuclei (DAPI, blue) in control mice
823 (left) and mice subjected to chronic islet injury induced by STZ for 140 days (right).
824 Scale bars: 2500 μm. See Supplementary Videos 10 and 11.
825 **b,** Time-course imaging of sympathetic nerve regeneration following selective
826 sympathetic nerve ablation using intrapancreatic 6-hydroxydopamine (6-OHDA)
827 injection. Upper: significant sympathetic (TH, magenta) regeneration and restoration
828 of structured associations with islets (insulin, green) at days 47, 56, and 65 post-
829 denervation. Lower: impaired sympathetic regeneration at corresponding time points
830 in mice subjected to severe islet injury induced by STZ administration one day post-
831 denervation. Scale bars: 2500 μm. See Supplementary Videos 15-20.
832
833 **Figure 4. Reg-family proteins, particularly Reg2 and Reg3β, are prominently**
834 **upregulated in pancreatic islets following sympathetic denervation.**
835 **a,** Schematic illustration of laser-capture microdissection (LCM) procedure for
836 precise isolation of pancreatic islets from pancreas tissue on day 7 post-sympathetic
837 denervation for mRNA sequencing.
838 **b,** mRNA sequencing analysis of LCM-isolated islets revealed different expression
839 genes (DEGs) post-denervation (n = 3 per group).

840 **c,** Experimental workflow illustrating conventional isolation of pancreatic islets at
841 multiple time points (days 3, 7, 14, and 21) post-sympathetic denervation for RNA
842 sequencing analysis.
843 **d,** mRNA sequencing-based temporal expression profiles of Reg-family genes in
844 conventionally isolated islets post-denervation (n = 3 per group per time point).
845 **e,** Real-time quantitative PCR (RT-qPCR) validation of *Reg2 and Reg3b* expression at
846 indicated time points using samples from (d) (n = 3 per group per time point). Data
847 presented as mean ± SEM, analyzed by two-tailed Student's t-test. *$P < 0.05$, **$P <$
848 0.01, ***$P < 0.001$.
849
850 **Figure 5. Exogenous rReg2 and rReg3β enhance sympathetic nerve regeneration**
851 **and improve functional outcomes in transplanted islets.**
852 **a,** Representative whole-kidney clearing images (left) showing sympathetic nerves
853 (TH, magenta), transplanted islets (insulin, green) at day 50 post-transplantation.
854 Corresponding 3D reconstructions (right) illustrate pre-existing renal sympathetic
855 nerves (magenta), islet-recruited sympathetic nerves (yellow), transplanted islets
856 (green), and the adrenal gland (blue). White arrowheads indicate sympathetic nerves
857 extending toward islets. Recombinant regenerating protein 2 (rReg2) and recombinant
858 regenerating protein 3 beta (rReg3β) proteins were incorporated into hydrogel during
859 gelation, thereby achieving localized drug delivery to islet grafts. Scale bar, 1000 μm.
860 See Supplementary Video 24.

861 **b,** Quantification of sympathetic nerve fibers extending toward transplanted islets
862 following localized hydrogel delivery of rReg2 and rReg3β proteins, as illustrated in
863 (a) (n = 4 per group).
864 **c,** Representative whole-kidney clearing images (left) at day 35 post-transplantation
865 showing sympathetic nerves (TH, magenta), transplanted islets (insulin, green).
866 Corresponding 3D reconstructions (right) illustrate pre-existing renal sympathetic
867 nerves (magenta), islet-recruited sympathetic nerves (yellow), transplanted islets
868 (green), and the adrenal gland (blue). White arrowheads indicate sympathetic nerves
869 extending toward islets. rReg2 and rReg3β proteins were systemically administered
870 via intraperitoneal (i.p.) injections on days 1, 3, and 5 post-transplantation. Scale bar,
871 1000 μm. See Supplementary Video 25.
872 **d,** Quantification of sympathetic nerve fibers extending toward transplanted islets
873 following i.p. injection of rReg2 and rReg3β proteins, as illustrated in (c) (n = 3 per
874 group).
875 **e,** Representative whole-kidney clearing images (left) at day 60 post-transplantation
876 showing sympathetic nerves (TH, magenta) and transplanted islets (insulin, green).
877 Corresponding 3D reconstructions (right) illustrate pre-existing renal sympathetic
878 nerves (magenta), islet-recruited sympathetic nerves (yellow), transplanted islets
879 (green), and adrenal gland (blue), following lentiviral-mediated knockdown of *Reg2*
880 and *Reg3b*. White arrowheads indicate sympathetic nerves extending toward islets.
881 Knockdown efficiency was verified by RT-qPCR (Supplementary Fig.5d); shRNA

882 sequences provided in Supplementary Table 1. Scale bar, 1000 μm. See
883 Supplementary Video 26.
884 **f,** Quantification of sympathetic nerve fibers extending toward transplanted islets
885 following lentiviral-mediated knockdown of *Reg2* and *Reg3b*, as illustrated in (e) (n =
886 3 per group).
887 **g, h,** IPGTT at days 30 (g) and 50 (h) post-transplantation. Notably, the enhancement
888 in islet graft function was more pronounced at day 50 than at day 30 (n = 3-4 per
889 group per time point). Corresponding whole-kidney clearing images are shown in
890 Supplementary Video 27.
891 Data are shown as mean ± SEM, analyzed by two-tailed Student's t-test. *$P < 0.05$,
892 **$P < 0.01$, ***$P < 0.001$.
893
894

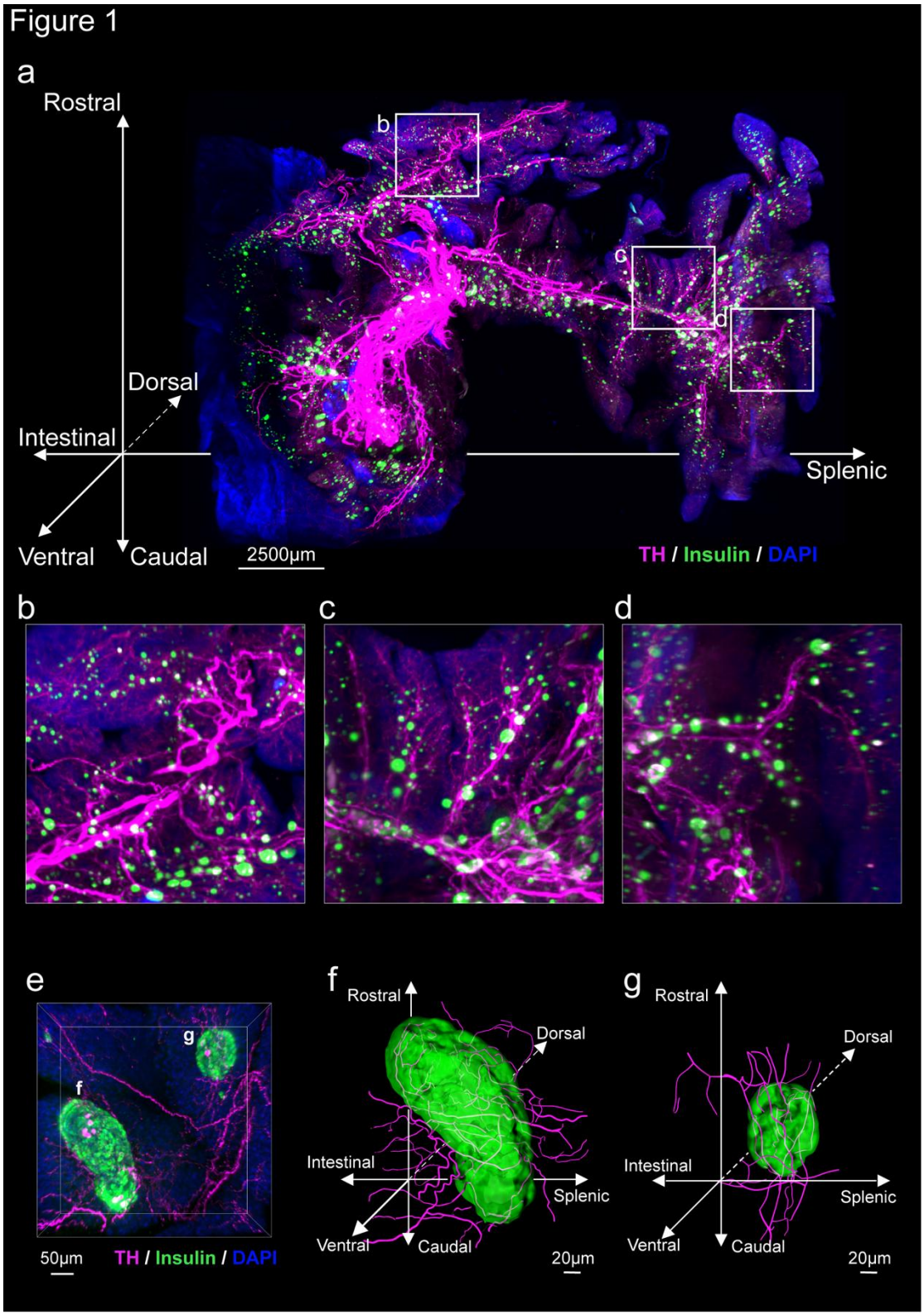
Figure 1
a
Rostral
Dorsal
Intestinal
Ventral
Caudal
Splenic
b
c
d
2500µm
TH / Insulin / DAPI
b
c
d
e
f
g
50µm
TH / Insulin / DAPI
f
Rostral
Dorsal
Intestinal
Splenic
Ventral
Caudal
20µm
g
Rostral
Dorsal
Intestinal
Splenic
Ventral
Caudal
20µm

895

Figure 2

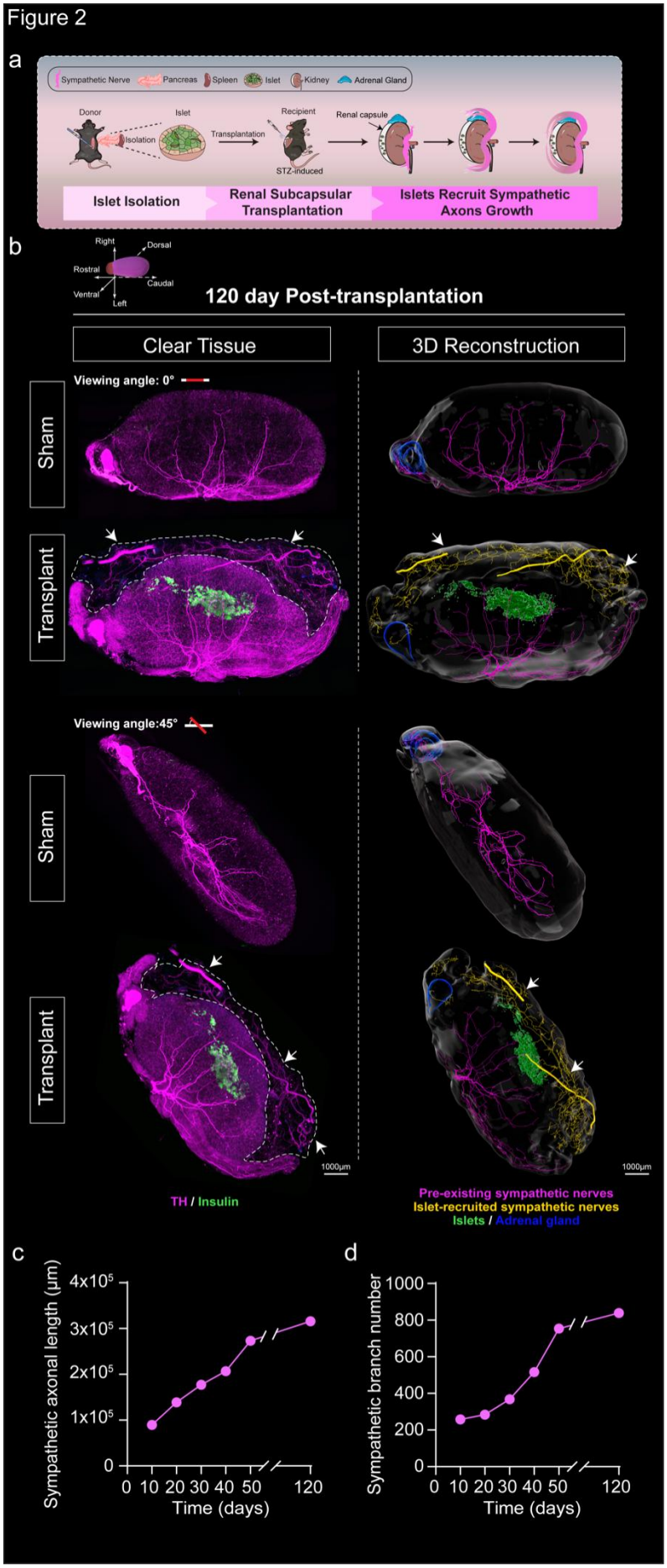
a
Sympathetic Nerve
Pancreas
Spleen
Islet
Kidney
Adrenal Gland
Donor
Islet
Isolation
Transplantation
Recipient
STZ-induced
Renal capsule
Islet Isolation
Renal Subcapsular Transplantation
Islets Recruit Sympathetic Axons Growth
b
Right
Dorsal
Rostral
Caudal
Ventral
Left
120 day Post-transplantation
Clear Tissue
3D Reconstruction
Viewing angle: 0°
Sham
Transplant
Viewing angle:45°
Sham
Transplant
1000μm
1000μm
TH / Insulin
Pre-existing sympathetic nerves
Islet-recruited sympathetic nerves
Islets / Adrenal gland
c
Sympathetic axonal length (μm)
4x10^5
3x10^5
2x10^5
1x10^5
0
0 10 20 30 40 50 120
Time (days)
d
Sympathetic branch number
1000
800
600
400
200
0
0 10 20 30 40 50 120
Time (days)

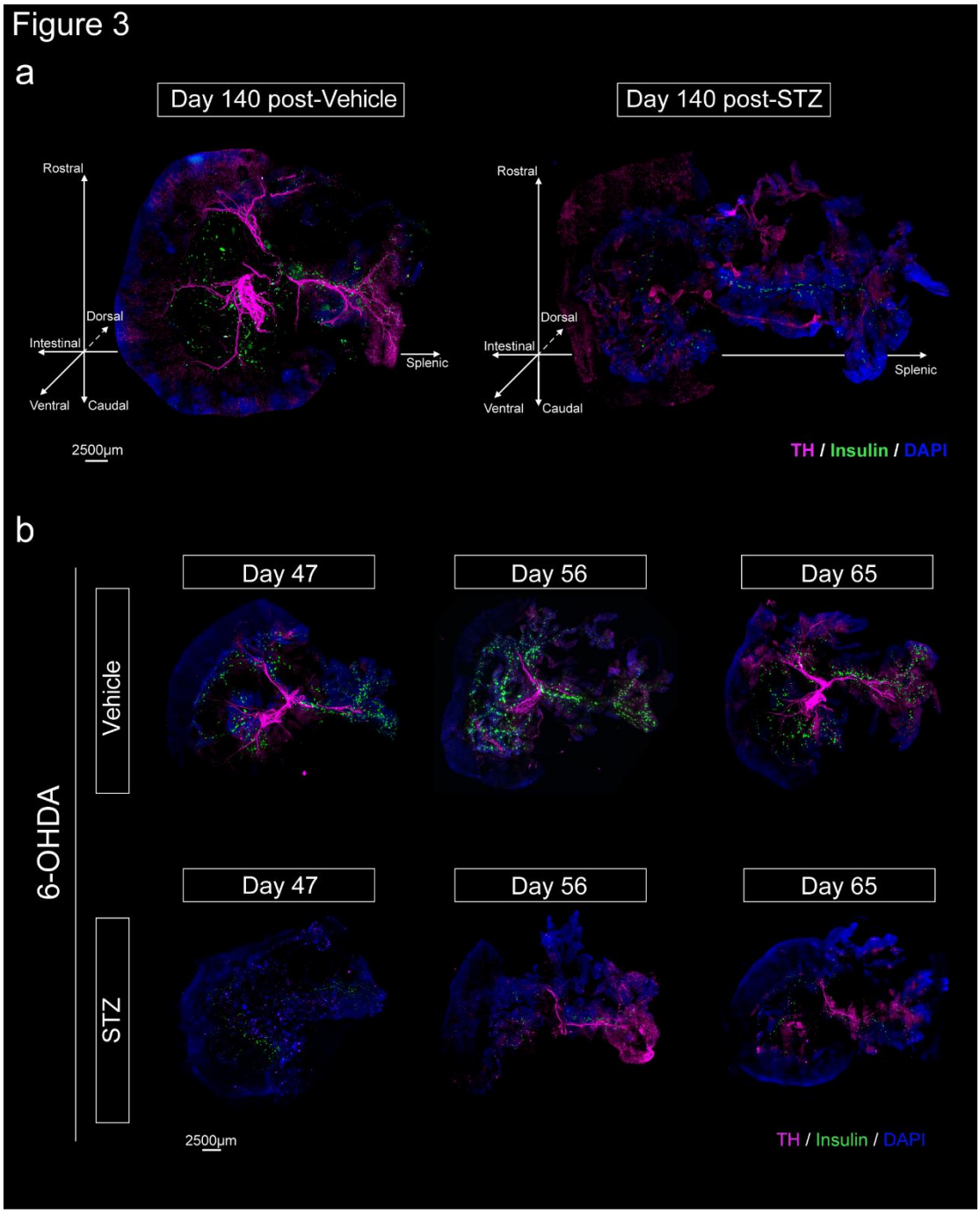
Figure 3
a
Day 140 post-Vehicle
Day 140 post-STZ
Rostral
Dorsal
Intestinal
Ventral
Caudal
Splenic
2500µm
TH / Insulin / DAPI
b
6-OHDA
Vehicle
STZ
Day 47
Day 56
Day 65
2500µm
TH / Insulin / DAPI

897

Figure 4

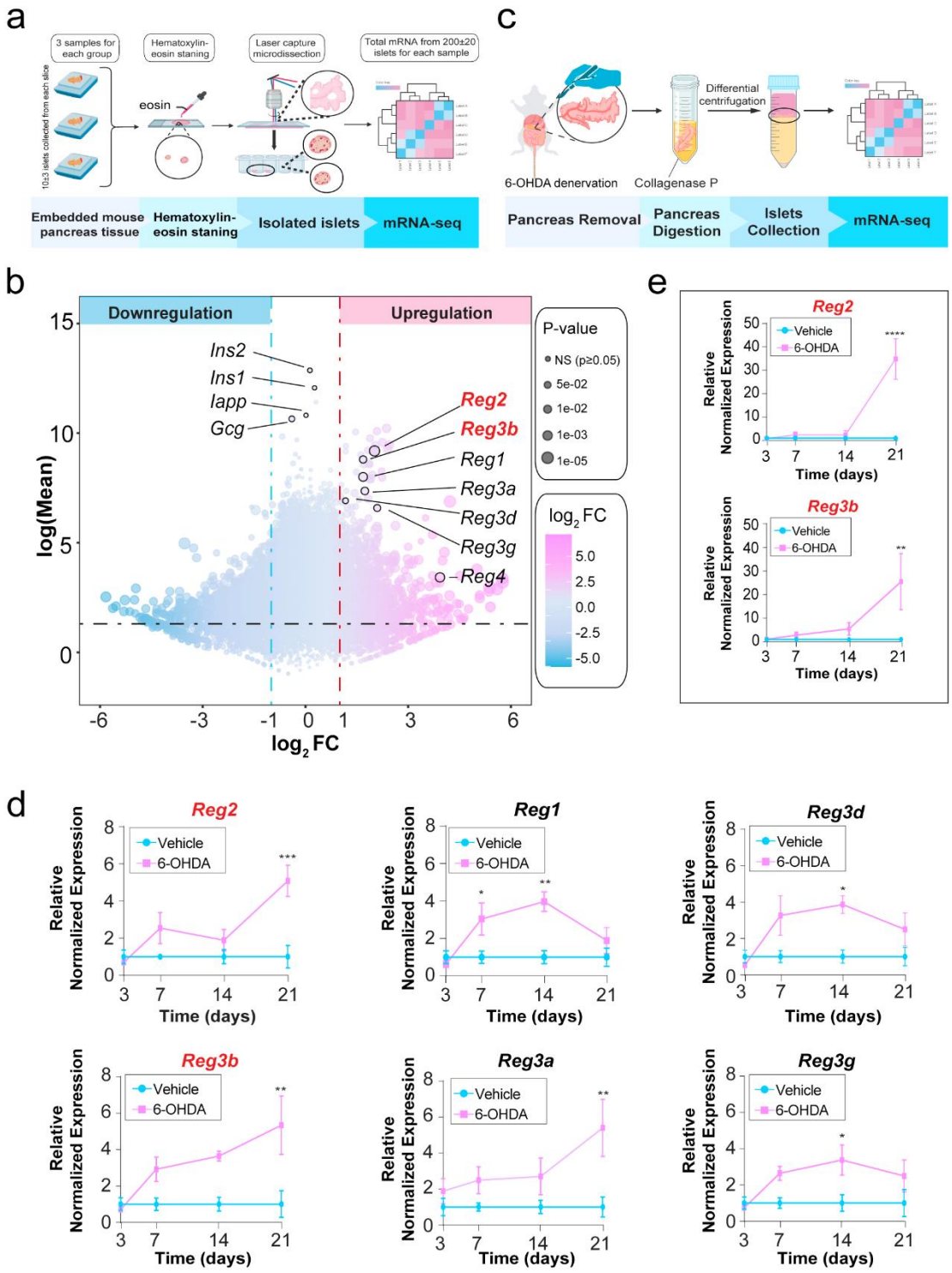
a
3 samples for each group
Hematoxylin-eosin staning
Laser capture microdissection
Total mRNA from 200±20 islets for each sample
10±3 islets collected from each slice
eosin
Embedded mouse pancreas tissue
Hematoxylin-eosin staning
Isolated islets
mRNA-seq
c
6-OHDA denervation
Collagenase P
Differential centrifugation
Pancreas Removal
Pancreas Digestion
Islets Collection
mRNA-seq
b
Downregulation
Upregulation
Ins2
Ins1
Iapp
Gcg
Reg2
Reg3b
Reg1
Reg3a
Reg3d
Reg3g
Reg4
P-value
NS (p≥0.05)
5e-02
1e-02
1e-03
1e-05
log2 FC
5.0
2.5
0.0
-2.5
-5.0
log(Mean)
log2 FC
e
Reg2
Reg3b
Vehicle
6-OHDA
Relative Normalized Expression
Time (days)
d
Reg2
Reg1
Reg3d
Reg3b
Reg3a
Reg3g

898

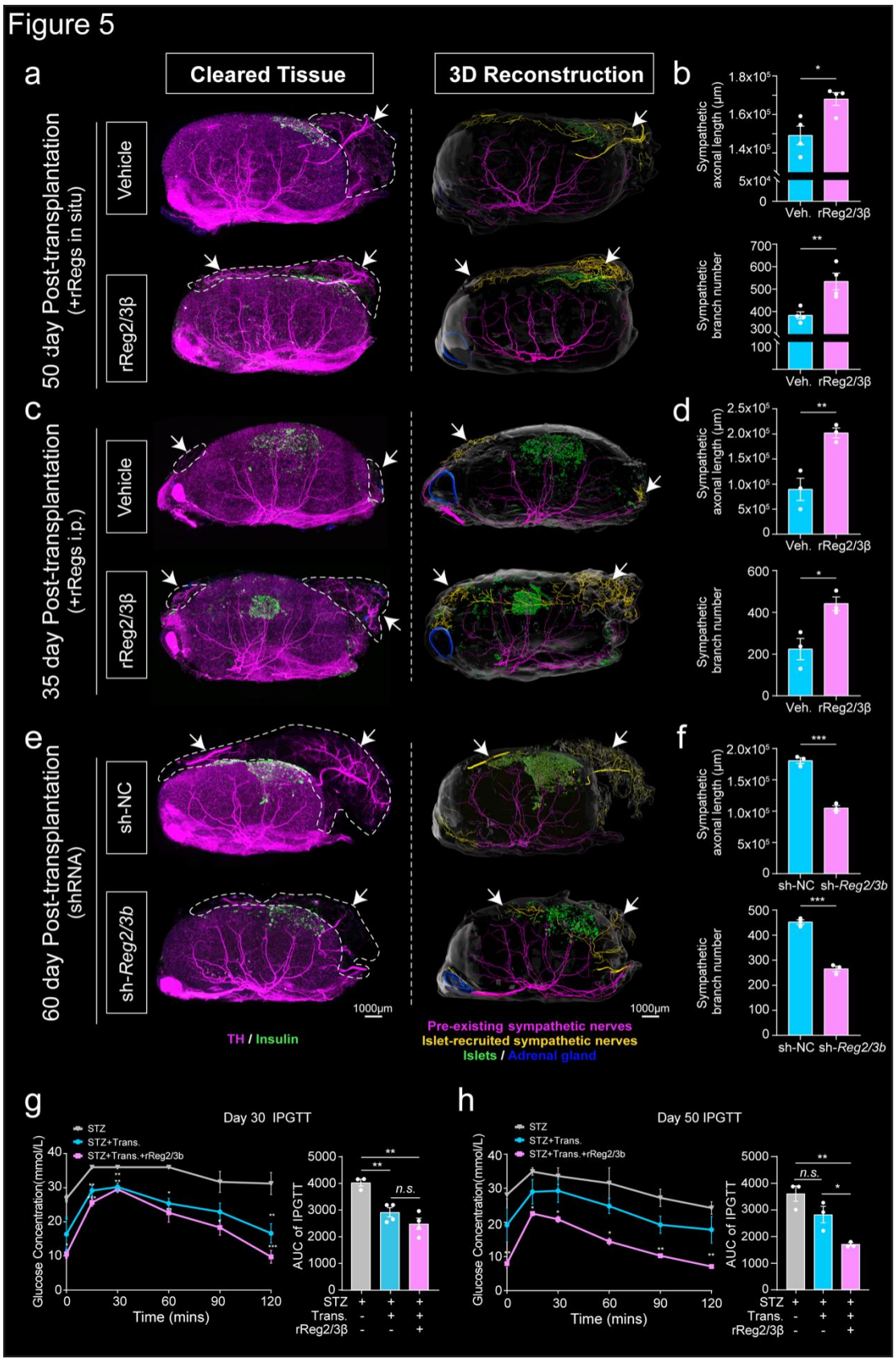
Figure 5
a
Cleared Tissue
3D Reconstruction
b
50 day Post-transplantation
(+rRegs in situ)
Vehicle
rReg2/3β
Sympathetic axonal length (μm)
Sympathetic branch number
Veh.
rReg2/3β
c
d
35 day Post-transplantation
(+rRegs i.p.)
e
f
60 day Post-transplantation
(shRNA)
sh-NC
sh-Reg2/3b
1000μm
TH / Insulin
Pre-existing sympathetic nerves
Islet-recruited sympathetic nerves
Islets / Adrenal gland
g
Day 30 IPGTT
STZ
STZ+Trans.
STZ+Trans.+rReg2/3b
Glucose Concentration(mmol/L)
Time (mins)
AUC of IPGTT
n.s.
Trans.
h
Day 50 IPGTT

899